An opto-electro-mechanical infrared photon detector with high internal gain at room temperature

John Kohoutek, Ivy Yoke Leng Wan, Omer Gokalp Memis, Hooman Mohseni*

Bio-Inspired Sensors and Optoelectronics Laboratory (BISOL), EECS, Northwestern University
2145 Sheridan Rd., Evanston, IL,USA, 60208
**hmohseni@ece.northwestern.edu*

Abstract: Many applications require detectors with both high sensitivity and linearity, such as low light level imaging and quantum computing. Here we present an opto-electro-mechanical detector based on nano-injection and lateral charge compression that operates at the short infrared (SWIR) range. Electrical signal is generated by photo-induced changes in a nano-injector gap, and subsequent change of tunneling current. We present a theoretical model developed for the OEM detector, and it shows good agreement with the measured experimental results for both the mechanical and electrical properties of the device. The device shows a measured responsivity of 276 A/W, equivalent to 220 electrons per incoming photon, and an NEP of 3.53 $\times$ 10^{-14} W/Hz$^{0.5}$ at room temperature. Although these results are already competing with common APDs in linear mode, we believe replacing the AFM tip with a dedicated nanoinjector can improve the sensitivity significantly.

OCIS codes: (040.3780) Low light level detectors; (230.4685) Optical microelectromechanical devices; (230.5160) Photodetectors

References and links

1. T. J. Kippenberg, and K. J. Vahala, "Cavity optomechanics: back-action at the mesoscale," Science **321**(5893), 1172–1176 (2008).
2. T. C. Tsu, "Interplanetary Travel by Solar Sail," ARS J. **29**(6), (1959).
3. C. H. Metzger, and K. Karrai, "Cavity cooling of a microlever," Nature **432**(7020), 1002–1005 (2004).
4. O. Arcizet, P. F. Cohadon, T. Briant, M. Pinard, and A. Heidmann, "Radiation-pressure cooling and optomechanical instability of a micromirror," Nature **444**(7115), 71–74 (2006).
5. M. Li, H. X. Tang, and M. L. Roukes, "Ultra-sensitive NEMS-based cantilevers for sensing, scanned probe and very high-frequency applications," Nat. Nanotechnol. **2**(2), 114–120 (2007).
6. A. C. Bleszynski-Jayich, W. E. Shanks, B. R. Ilic, and J. G. E. Harris, "High sensitivity cantilevers for measuring persistent currents in normal metal rings," J. Vac. Sci. Technol. B **26**(4), 1412 (2008).
7. H. Mohseni, J. Wojkowski, and M. Razeghi, "Uncooled InAs-GaSb type-II infrared detectors grown on GaAs substrates for the 8-12-mu m atmospheric window," IEEE J. Quantum Electron. **35**(1041), (1999).
8. J. C. Campbell, "Recent advances in telecommunications avalanche photodiodes," J. Lightwave Technol. **25**(1), 109–121 (2007).
9. L. Aina, *et al*., "Linear-mode single photon counting APD arrays with subnanosecond, afterpulse-free performance for ladar, spectroscopy, and QKD applications," Proc. SPIE **6572**, 65720H–1 (2007).
10. O. G. Memis, A. Katsnelson, S.-C. Kong, H. Mohseni, M. Yan, S. Zhang, T. Hossain, N. Jin, and I. Adesida, "A photon detector with very high gain at low bias and at room temperature," Appl. Phys. Lett. **91**(17), 171112 (2007).
11. O. G. Memis, A. Katsnelson, H. Mohseni, M. Yan, S. Zhang, T. Hossain, N. Jin, and I. Adesida, "On the Source of Jitter in a Room-Temperature Nanoinjection Photon Detector at 1.55 μm," IEEE Electron Device Lett. **29**(8), 867–869 (2008).
12. O. G. Memis, A. Katsnelson, S. C. Kong, H. Mohseni, M. Yan, S. Zhang, T. Hossain, N. Jin, and I. Adesida, "Sub-Poissonian shot noise of a high internal gain injection photon detector," Opt. Express **16**(17), 12701–12706 (2008).
13. P. L. Voss, *et al*., "14MHz rate photon counting with room temperature InGaAs/InP avalanche photodiodes," J. Mod. Opt. **51**(9–10), 1369–1379 (2004).

#110975 - $15.00 USD Received 5 May 2009; revised 16 Jul 2009; accepted 18 Jul 2009; published 3 Aug 2009

14. U. Mohideen, and A. Roy, "Precision measurement of the Casimir force from 0.1 to 0.9 μm," Phys. Rev. Lett. **81**(21), 4549–4552 (1998).
15. J. N. Munday, F. Capasso, and V. A. Parsegian, "Measured long-range repulsive Casimir-Lifshitz forces," Nature **457**(7226), 170–173 (2009).
16. H. B. Chan, V. A. Aksyuk, R. N. Kleiman, D. J. Bishop, and F. Capasso, "Quantum mechanical actuation of microelectromechanical systems by the Casimir force," Science **291**(5510), 1941–1944 (2001).
17. F. Chen, *et al*., "Measurements of the normal and shape dependent Casimir forces using an Atomic Force Microscope," Int. J. Mod. Phys. A **17**(6&7), 711–721 (2002).
18. A. Roy, C. Y. Lin, and U. Mohideen, "Improved precision measurement of the Casimir force," Phys. Rev. D Part. Fields **60**(11), 111101 (1999).
19. P. S. Maruvada, and N. Hylten-Cavallius, "Capacitance Calculations for Basic High Voltage Electrode Configurations," IEEE Trans. Power Apparatus Syst **PAS-94**(5), (1975).

1. Introduction

Using light to sense mechanical changes is something that has been done ever since Michelson built his famous interferometer in 1887. However, using mechanical changes to sense light is relatively new. The concept of opto-mechanical coupling has been explored in many applications [1] such as solar sails for space propulsion [2] and more recently radiation cooling [3,4]. One of the most sensitive ways to detect light mechanically is to use a vibrating MEMS-based cantilever (e.g. atomic force microscopy) and the exchange of the photon momentum to sense the force exerted by the light directly [3]. In that case, the maximum force exerted by the light will be the power of the light divided by the speed of light, giving an opto-mechanical conversion factor of about 3.3×10^{-9} Newton per Watt of optical power. The minimum measureable force with this method, limited by the Brownian motion of the cantilever, can be calculated using: $F_{\min} = \sqrt{\frac{4k_B TkB}{\omega_0 Q}}$, where k_B is the Boltzmann constant, T is the temperature, B is the bandwidth of the measurement, ω_0 is the resonance frequency, k is the spring constant, and Q is the quality factor of the cantilever [5,6]. For some modern cantilevers the value of F_{min} can be on the order of 5×10^{-16} N/Hz$^{0.5}$ at room temperature [6]. Therefore, the minimum detectable optical power, using the exchange of the photon reflected by a mirror, is about $F_{min} \cdot c/2 \sim 7.5 \times 10^{-8}$ Watt/Hz$^{0.5}$ at room temperature. Interestingly, this so-called noise equivalent power (NEP) of an opto-mechanical photon detector is completely wavelength independent. Nonetheless, it is about three orders of magnitude less sensitive than conventional photon detectors, even at long wavelengths infrared (LWIR) at room temperature [7].

2. Device concept

The detector we present here uses opto-electro-mechanical coupling with a conventional AFM in ambient conditions and achieves an NEP of 3.53×10^{-14} W/Hz$^{0.5}$ (see *Meaurement* section for NEP measurement). For comparison, a SWIR-detecting avalanche photodiode (APD) operating in the linear regime has an NEP on the same order, of about ~5×10^{-14} W/Hz$^{0.5}$ [8,9]. The basis for our detector comes from earlier work our group has done on a detector that involves a large absorbing region with a nanoinjecting sensing region [10–12]. The original detector has a large InGaAs absorbing area, capped by a thin layer of GaAsSb which acts as a trap for holes. On the top of the detector is a small pillar of InP, which acts as a nanoinjector where the charge density increases dramatically. In the new detector, we replace the static InP nanoinjector with a moving AFM tip. A model of the detector can be seen in Fig. 1(a). The surface potential created by photo-generated holes trapped in the GaAsSb layer makes a capacitive force on the AFM tip, pulling it closer to the surface. More importantly, the electric field between the tip and the surface has a focusing effect on the photo-generated holes in the semiconductor, creating a small region of high charge density right beneath the tip. Plots showing the electric field and surface charge density versus radial distance are shown in Fig. 1. As we demonstrated earlier, this charge compression has profound effects,

#110975 - $15.00 USD Received 5 May 2009; revised 16 Jul 2009; accepted 18 Jul 2009; published 3 Aug 2009

including enhancement of detector efficiency and sensitivity [10]. The device relies on tunneling through an air gap for electrical signal. Because tunneling current between the surface and the tip is exponentially dependent on distance, the ratio of the photo-current to dark current (signal to noise) can be significantly enhanced, since the air gap is changing. Our measurement setup, detailed in the following, allow us to measure both the tunneling current and the movement of the nano-injector (AFM tip) simultaneously. In particular, we use the data from amplitude and phase of vibration to characterize the tip and the forces exerted on the tip. These parameters are then used in the presented opto-electro-mechanical model, which shows excellent agreement with the experimental data.

Now that we have an idea of how the detector works, we can make a simple theory for the optical power to force conversion factor and therefore the NEP. We have already seen that the NEP is simply the F_{min} divided by this conversion factor. For two parallel plates, the electrostatic force between them is simply:

$$F_{electrostatic} = -\frac{1}{2}\frac{dC}{dz}V^2 = \frac{1}{2}\frac{\varepsilon_0 A V^2}{d^2} = \frac{1}{2}\frac{Q^2}{\varepsilon_0 A} \tag{1}$$

where C is the capacitance, V is the voltage, A is the area of the plates, d is the distance between the plates, Q is the charge on the plates, and ε_0 is the permittivity of free space. We then know that:

$$dF = \frac{1}{\varepsilon_0 A} Q \cdot dQ = \frac{V}{d} \cdot dQ \tag{2}$$

The change in charge dQ can be taken to be:

$$dQ = \frac{q \cdot dP \cdot \tau \cdot \lambda}{\hbar c} \tag{3}$$

which is the incremental charge change for a given incremental change in incident optical power (dP), where q is the electron charge, τ is the carrier lifetime, λ is the wavelength, $\hbar$ is the reduced Planck's constant and c is the speed of light. This gives us:

$$dF/dP = \frac{Vq\tau\lambda}{d\hbar c} \tag{4}$$

which for our experimental parameters (V = 1.6 V, τ~100 ns, d~50 nm, λ = 1.55 μm), gives a conversion factor of 3.99 $(m/s)^{-1}$. If one uses the hemisphere/plate geometrical approximation used later in this paper, one arrives at a similar figure of 2.42 $(m/s)^{-1}$, using R~100 nm. This opto-electro-mechanical conversion factor is roughly 10^8 times higher than the opto-mechanical conversion factor of $2/c$ for an opto-mechanical detector presented earlier, and leads to an NEP of about $F_{min}/2.42 = 2 \times 10^{-16}$ $W/Hz^{0.5}$, which can be low enough to detect single photons, given the bandwidth of the measurement is high enough [13].

Our setup shown in Fig. 2(a) is quite similar to a Kelvin probe force microscope (KPFM) setup. Here we have the device under test, which is either our detector or a polished metallic surface for calibration, the procedure for which will be explained in the measurement section, mounted under the vibrating AFM tip. To calibrate the tip and measure its electro-mechanical properties, we directly applied modulated voltage to the tip with the function generator. For the opto-electro-mechanical measurements however, we applied modulated laser light to the sample, which deforms the surface potential. We feed the phase output of the AFM controller to an oscilloscope and lock-in amplifier. This allows us to sense the phase change of the tip at the frequency of applied voltage or light.

#110975 - $15.00 USD Received 5 May 2009; revised 16 Jul 2009; accepted 18 Jul 2009; published 3 Aug 2009

It is in observing this phase change that we believe we are able to see the effects of the quantum mechanical Casimir force. Since the late 1990's, research has been done using AFMs to measure the Casimir force [14–18]. These measurements have been performed with large metal spheres and/or flat metal plates. Here we observe the effects of Casimir force on conventional AFM tips, because its inclusion in the following model yield different results which agree much more accurately with what we observe, and can give an estimate on the magnitude of the Casimir force which is comparable to that of the electrostatic force.

3. Modeling

We have modeled the vibrating tip with the equation of motion for a forced, damped, harmonic oscillator with electrostatic force and Casimir force terms added:

$$m\frac{d^2x}{dt^2} + r\frac{dx}{dt} + kx = F_0 Cos(\omega_0 t) + F_{electrostatic} + F_{Casimir} \tag{5}$$

The parameters in this equation are the mass *m,* the damping *r,* the spring constant *k,* and the driving force F_0 . Here, *k* is given by the manufacturer of the AFM tip to be 3 N/m. The mass and damping factor are extracted from actual frequency response of the disengaged tip. Also F_0 was extracted from the measured amplitude of oscillation. The capacitance of the tip above the surface is approximated by the capacitance of a sphere above a plate which is given approximately by $C = 2\pi R\varepsilon_0 \ln(1 + R/d)$, with *R* the radius of curvature of the sphere, ε_0 the permittivity of free space, and *d* the distance between the plate and the sphere [19].

$F_{electrostatic}$ is then given by:

$$F_{electrostatic} = -\frac{1}{2}\frac{dC}{dz}V^2 = \frac{\pi R\varepsilon_0\left(V_{dc}^{\ 2} + 2V_{dc}V_{ac} + V_{ac}^{\ 2}\right)}{(d-x)^2/R + (d-x)} \tag{6}$$

where V_{dc} the DC voltage between the tip and surface, and V_{ac} the AC peak to peak voltage between the tip and surface. This formula has less than 5% error with our parameters compared with the exact formula given by [14]. $F_{Casimir}$ is given for a perfectly conducting sphere above a perfectly conducting plate by [14]:

$$F_{Casimir} = \frac{\pi^3}{360}R\frac{\hbar c}{(d-x)^3} \tag{7}$$

where $\hbar$ is Planck's constant, and *c* the speed of light. *R* was measured with a scanning electron microscope (SEM) to be around 113 nm. This leaves the only free parameter *d*.

4. Measurement

The devices were tested in a modified AFM setup as depicted in Fig. 2(a). We have measured the phase signal from a lock-in amplifier locked to the phase signal of the AFM tip for different incident optical powers, DC voltages applied to the tip, and frequencies of applied laser light or tip voltages. All measurements were done at room temperature and pressure. Solving the above differential equation numerically showed good agreement with the measured data (see Fig. 2(b)). We have used two different methods to estimate the unknown parameter, *d*, using the time response of the phase, indicating that the true *d* is somewhere very close to 50 nm.

Once we had all of the cantilever parameters, we could characterize the opto-electrial properties of the device by finding the surface potential as a function of absorbed optical power. To measure the surface potential as a function of absorbed optical power, we first shone laser light of differing optical power on the detector and recorded the phase signal output from the lock-in amplifier. Then, we removed the detector and replaced it with a grounded, polished metal plate. We applied AC voltages with different peak-to-peak

#110975 - $15.00 USD Received 5 May 2009; revised 16 Jul 2009; accepted 18 Jul 2009; published 3 Aug 2009

amplitudes to the tip while using the metal piece as the device under test. We then correlated the phase change caused by the different peak to peak amplitudes of the function generator with the different optical powers sent by the laser. As seen in Fig. 2(c) the detector begins to saturate at higher power. We have measured a surface potential of 155 mV with a maximum absorbed power of 2.8 nW, down to a surface potential of 1 mV with an absorbed power of 6.7 pW with this method.

Finally, we have recorded the tunneling current results produced by operating the AFM in constant-current Scanning Tunneling Microscopy (STM) mode with a conducting AFM cantilever/tip, since conventional STM tips are rigid. For the STM measurement, we have measured the current signal at different STM setpoints and different optical powers of the laser. The peak-to-peak signal as a function of absorbed optical power and STM setpoint is plotted in Fig. 3(a). We have calculated the bandwidth of this detection method, by measuring the frequency spectrum, to be 1.7 kHz at 67 pW. We have plotted the peak to peak current of the signal vs. setpoint and absorbed power in Fig. 3. The measurements taken in Fig. 3 were done with the tip positioning feedback loop off as to not interfere with the mechanical coupling. As such, the time for a stable measurement was reduced due to absence of feedback. Therefore, an average measurement was taken for the composite Fig. 3. One will also note that the responsivity at any point on this plot is the value of the peak to peak signal in Amps over the absorbed optical power in Watts. The peak responsivity and therefore gain appears at the highest setpoint, 20 nA. At this setpoint and at 67 pW, the responsivity is about 276 A/W and the gain is about 220 electrons per incident photon. For comparison, the typical gain of an InP/InGaAs based APD in linear mode is about 10 [8]. We have measured a minimum absorbed power of 335 fW and still seen our peak in the spectrum with this method. We have used these measurements to calculate the NEP of our device, of 3.53×10^{-14} W/Hz$^{0.5}$. To measure the NEP we measured the current as a function of time with no optical illumination and then looked at the spectrum of this measurement to extract the noise spectral density in A/Hz$^{0.5}$. We then divided this number by the responsivity to arrive at our NEP in Watts/Hz$^{0.5}$. The device, with a dark current of 20 nA, was not limited by the shot noise, since the NEP due to shot noise is $\sqrt{2I_{dark}qG}/R = 4.3 \times 10^{-15}$ A/Hz$^{0.5}$ where q is the electron charge, G is the gain, and R is the responsivity [12].

We have also used a three-dimensional finite element method (FEM) simulation of the device and simulated the surface potential as a function of incident power. The results of the simulation shows a better than factor of 3.5 agreement with experiment for optical power greater than 10^{-11} W. The source of this error could be that our device is not fully optimized, and also that we have only used nominal values for carrier lifetime and band alignment from the literature, which report a wide range of values for these parameters. Our simulation also does not include surface charge effects due to the termination of the surface. The results of this simulation are pictured in Fig. 2(c) and in Fig. 1.

5. Conclusion

We believe that these results provide the proof-of-principle for a novel opto-electro-mechanical (OEM) nano-injection detector. This detector operates on the principle effect of the focusing of charge and electric field by the tip, which is compelled to move under the electrostatic force created by the incoming light. Experimentally, we have shown that the tip is indeed influenced by this force mechanically, even for very low optical power. We have also shown tunneling current results that prove that a realistic photon detector can operate on this principle. Finally, we have created a theoretical model for the mechanical motion of the tip. We have used the equation of motion for a forced, damped, harmonic oscillator with electrostatic and Casimir force terms added to model the vibrating AFM tip. Results of phase vs. time agree well with experiment, and our theoretical model only has one free parameter, the distance of the tip to the surface. We have compared the results for gain and NEP of this

#110975 - $15.00 USD Received 5 May 2009; revised 16 Jul 2009; accepted 18 Jul 2009; published 3 Aug 2009

prototype with those of an SWIR-detecting APD operated in linear mode. The detector described here shows a gain of 220 electrons per photon versus the typical gain of ~10 for a linear mode APD while the two devices have comparable NEP. With custom processing, these devices might approach the theoretical limit to detect single photons with the ability to do so at room temperature.

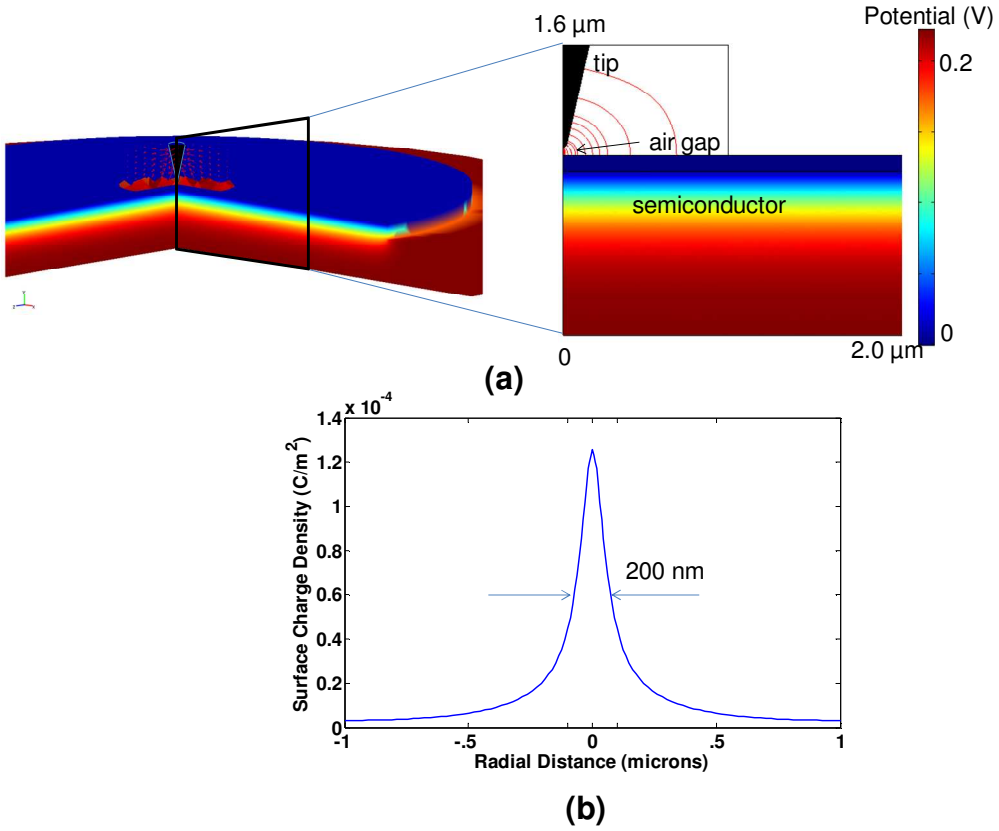

Fig. 1. (a). 3-D Finite Element Method (FEM) simulation of a metal tip 45 nm above a specialized detector device, shown is the potential within the semiconductor of the detector, the tip in black, and the equipotential surfaces. Inset is shown a cross-section of the 3-D view. 1(b). Surface charge density as a function of radial distance for a metal tip 45 nm above a semiconductor surface with a −1 V bias applied to the tip. Most of the charge is focalized in a 200 nm diameter area.

#110975 - $15.00 USD Received 5 May 2009; revised 16 Jul 2009; accepted 18 Jul 2009; published 3 Aug 2009

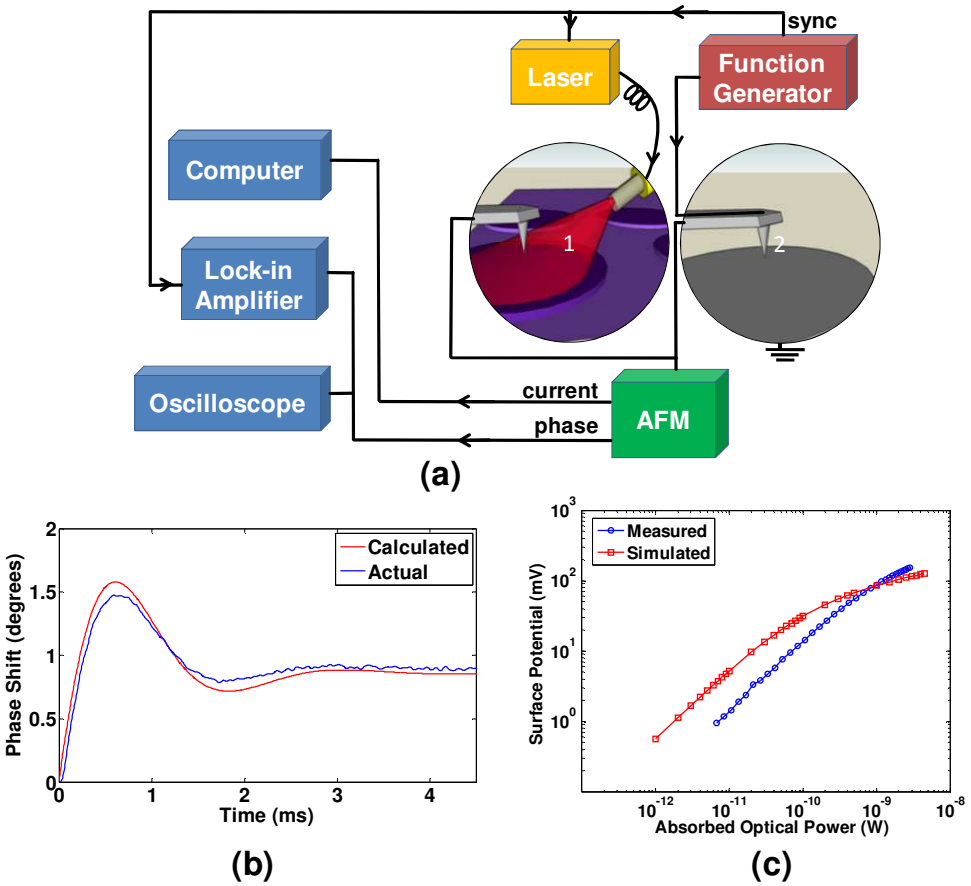

Fig. 2. Experimental setup and results. 2(a). Experimental setup showing both configurations. 2(b). Calculated and actual phase shift of AFM tip as a function of time when tip bias is turned on at time t = 0. 2c. Surface potential vs. Absorbed optical power, both measured and simulated results are given.

#110975 - $15.00 USD Received 5 May 2009; revised 16 Jul 2009; accepted 18 Jul 2009; published 3 Aug 2009

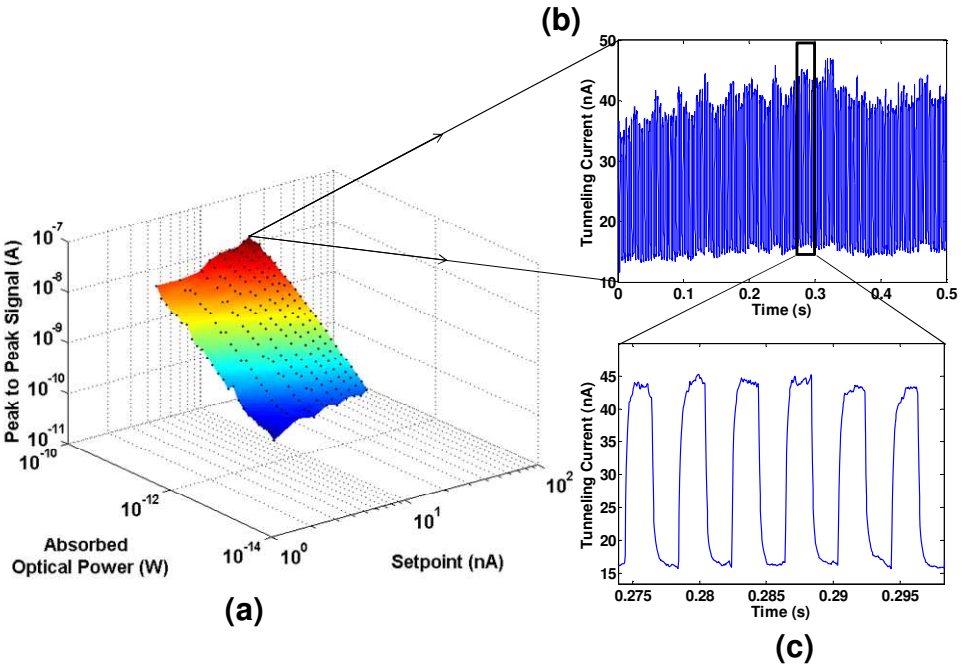

Fig. 3. (a). Peak to peak current as a function of absorbed optical power and STM setpoint. The responsivity at a given setpoint is the value of the peak to peak signal in Amps over the absorbed optical power in Watts. 3(b). Tunneling current as a function of time over a single measurement, for a single setpoint and single incident power. 3c. Zoomed in section of 3(b).

#110975 - $15.00 USD Received 5 May 2009; revised 16 Jul 2009; accepted 18 Jul 2009; published 3 Aug 2009